RSC Advances

PAPER

View Article Online
View Journal | View Issue

Cite this: *RSC Adv.*, 2020, **10**, 41857

A functional modified graphene oxide/nanodiamond/nano zinc oxide composite for excellent vulcanization properties of natural rubber

Zhen Yang, [a] Yan Huang[a] and Yuzhu Xiong *[ab]

A modified graphene oxide/nanodiamond/nanozinc oxide (MGO/ND/nanoZnO) functional hybrid filler is designed and prepared to improve the vulcanization efficiency of a rubber composite and to reduce the use of ZnO. ND was grafted onto graphite oxide with the aid of 4,4′-methylene diphenyl diisocyanate (MDI). NanoZnO, with high surface activity, was then loaded onto the MGO/ND complex through the wet chemical method, in order to synthesize the MGO/ND/nanoZnO functional hybrid filler. Rubber composites were prepared using the rubber latex composite method and their vulcanization behaviors were investigated. Our results show that the MGO/ND/nanoZnO functional hybrid filler can remarkably improve the vulcanization behaviors of the rubber composite. Compared with that of pure natural rubber (NR), the vulcanization activation energy of the rubber composite was reduced by approximately 16%. Moreover, the vulcanization efficiency can be improved by 63% (*i.e.*, the optimum cure time is shortened from the original 405 s to 150 s) after the same amount of traditional ZnO was replaced by the functional hybrid filler loaded with 1 wt% nanoZnO. The prepared MGO/ND/nanoZnO functional hybrid filler thus provides a promising alternative to improve the vulcanization efficiency of rubber composites.

Received 28th August 2020
Accepted 11th November 2020

DOI: 10.1039/d0ra07404g

rsc.li/rsc-advances

1. Introduction

In-depth studies on rubber vulcanization behaviors and vulcanization kinetics have been conducted since the discovery of rubber vulcanization technology.[1–3] Coran pointed out that scorching is an important part of rubber vulcanization behavior. In this process,[4] various accelerants react with sulfur to form crosslinking precursors, which then react with active sites on the rubber chain during vulcanization to form S bonds between macromolecular chains. In order to better describe the vulcanizing and processing properties of NR, Ehabé *et al.* used Mooney torque relaxation method to characterize natural rubber and synthetic natural rubber, and found that the Maxwell and Wu–Abott models are most suitable for describing rubber vulcanization and processing performance.[5] Among them, according to the classification of the curing system, it is divided into three types: conventional (CV), semi-efficient (SEV), and efficient (EV) curing systems, the classification standard is the ratio of sulfur to accelerator. Generally, conventional curing systems have better mechanical properties.[6] In addition, ZnO also plays an important role in the vulcanization process. In the description of Mostoni *et al.*, ZnO participates as an activator in the vulcanization process of rubber, the activation process consists of three steps. First, forming a zinc complex with stearic acid and then forming an active accelerator complex with an accelerator and sulfur, and finally reacts with the polymer to form multiple sulfide crosslinked products. With the process of curing reaction, the polysulfide bonds will gradually break to form stable, short sulfur cross-links and finally form a stable 3D network structure.[7] Therefore, rubber vulcanization directly affects the quality of the 3D net structure, which supports various properties of the rubber material. In addition, the vulcanization behaviors of the rubber materials also directly influence their applications.

ZnO has been widely used in the vulcanization process of NR recently years. Owing to the strict requirements of EU REACH Regulations for the environmental protection property of traditional ZnO, many researchers have focused on reducing the use of traditional ZnO,[8] therefore, nanoZnO came into being. NanoZnO is a multifunctional material with extremely high surface activity. It has the characteristics of small particle size and large specific surface area, and has a good effect of promoting vulcanization.[9] Kim *et al.* mixed nanoZnO into natural/butadiene composite rubber materials. They found that, in the silica-filled system, the high specific surface area and good dispersion of nanoZnO significantly promoted the vulcanization behavior and reduced both the scorch time and optimum curing time. Compared with conventional ZnO, 20% nanoZnO content can obtain similar vulcanization characteristics and mechanical properties.[10] Thomas *et al.* and Roy *et al.* also found that nanoZnO increased the scorch time of rubber and reduced the optimum curing time. They inferred that this

[a]*College of Materials and Metallurgy, Guizhou University, Guiyang 550025, China. E-mail: xyzhu789@126.com*

[b]*Guizhou Provincial Rubber Composite Material Engineering Laboratory, China*

may be related to the formation of more crosslinked precursors, due to the high specific surface area of nanoZnO.[11,12]

Recent works have focused on the use of nanoZnO to partially or completely replace conventional ZnO for rubber vulcanization. Due to the nanometer effect of nanoZnO, it can significantly improve the vulcanization performance of rubber and the utilization rate of rubber vulcanizing agent with a small amount of addition.[13] However, nanoZnO has high surface activity; when it is added independently, intense aggregation may occur in the rubber matrix,[14] degrading the vulcanization-facilitating effect and adversely influencing the resulting mechanical properties. Therefore, it is particularly important to improve the dispersity of nanoZnO in the rubber matrix. Among the methods to improve the dispersion of nanoZnO, the most commonly used method is to load nanoZnO onto other functional fillers with good dispersion. Numerous studies have shown that loading nanoZnO particles on SiO_2 can form a Si–O–Zn covalent bond, and finally makes nanoZnO uniformly dispersed in the rubber matrix along with SiO_2, thereby improving the vulcanization efficiency of rubber.[15–17] Lin *et al.* loaded nanoZnO onto the surface of graphene and found that nanoZnO inhibits the aggregation of graphene sheets. The results show that this new hybrid filler had a better vulcanization-facilitating effect.[18] In addition, based on the assumption that increased availability of Zn^{2+} ions may result in a significant reduction of ZnO needed in rubber compounds, Heideman *et al.* used montmorillonite as a carrier to load Zn^{2+} ions through an ion exchange process to prepare a new type of vulcanization active agent, ZnClay. Studies have found that ZnClay can not only maintain the vulcanization and physical properties of rubber products of traditional ZnO, but also reduce the impact on the environment. Heideman *et al.* also found that GaO and MgO are suitable substitutes for ZnO.[19,20]

To improve the dispersion of nanoZnO in the rubber matrix by loading, it is crucial to select a suitable carrier material. As a derivative of graphene, graphene oxide (GO) contains hybridized carbon atoms with a 2D honeycomb structure; its surface is covered with abundant functional groups that react with numerous compounds. GO is a versatile functional material,[21,22] and researchers have noticed the role of GO in rubber vulcanization. Bismark *et al.* found that reduced GO (rGO) can effectively promote the vulcanization of acrylonitrile-butadiene rubber, because the rGO can be dispersed well in the rubber matrix.[23] Wu *et al.* investigated the effect of graphene addition on the vulcanization kinetics of natural rubber and found that the scorching period was shortened in the presence of graphene and the vulcanization rate was elevated under low graphene filling condition, but restricted under high filling condition; this phenomenon occurs as the basic groups on the graphene surface participate in the vulcanization.[24] The strong van der Waals (VDW) forces between GO sheets is essential for the GO-filled polymer material, but the large agglomerates in the polymer matrix hinder the role of GO.[25] Therefore, the dispersity of GO-reinforced polymers in the polymer matrix must be improved. Researchers have grafted macromolecular compounds onto GO sheets to inhibit their aggregation and improve their dispersity in the polymer matrix.[26,27] Another method to improve dispersity is to prepare hybrid materials. Delville *et al.* used chemical grafting to prepare a hybrid material composed of molecular/nanoscale organic–inorganic units. This material has the characteristics of chemical and structural diversity, which can effectively improve the performance of polymers.[28] Rattanasom *et al.* used a CB–silica dual phase filler to reinforce natural rubber and found that, when the silica percentage was 20%, the vulcanized rubber had better performance.[29] GO has a 2D structure, so other nanoparticles can be imported onto GO sheets to reduce their aggregation. Moreover, the surface of GO contains a large number of active groups, which can provide active sites to form hybrid fillers, it is very suitable as a carrier material.[30]

Nano-diamond (ND) is a suitable intercalation material for GO because of its unique surface structure, abundant active groups and excellent thermal conductivity and stability.[31] At the same time, this material can facilitate rubber vulcanization and epoxy resin curing.[32,33] Owing to the active groups on its surface, ND can form hybridized fillers through the modification of grafted macromolecular substances and reactions between groups. However, there are few reports on ND grafted GO. Zhao *et al.* successfully grafted hydroxylated and aminated ND onto the surface of carbon fiber by covalent bonding. The results showed that the specific surface area of carbon fiber was enlarged by 58%.[34] Because the particle size of ND is far smaller than GO sheet diameter, it is feasible to graft ND onto GO surface, and the hybrid of the two materials can greatly promote the vulcanization behavior of rubber.

In this work, we used GO as matrix, grafted ND particles onto GO sheets with coupling agent MDI and expanded the lamellar structure. The functional hybridized filler MGO/ND/nanoZnO was prepared through the *in situ* loading of nanoZnO onto the MGO/ND complex using the wet chemical method. Then, natural rubber and functional hybrid filler were mixed by rubber latex composite method. Using this method, drying of the obtained nanofiller in a hot oven or freeze dryer could be avoided; this can not only lower the production cost, but also prevent the aggregation of the hybrid materials.[35,36] Moreover, the latex compounding method can effectively disperse fillers in polymer matrix and has been widely used.[37] Finally, vulcanization behaviors, vulcanization kinetics, and mechanical properties of the resultant rubber composite are investigated, and the related action mechanism is discussed.

2. Experiment

2.1. Materials

Natural rubber (NR) with an average particle size of 1.06 μm and total solid content of 60% was provided by Shenzhen Jitian Chemical Co., Ltd. GO was acquired from Shenzhen Zhongsen Linghang Technology Co., Ltd. ND was obtained from Beijing Guoruisheng Co., Ltd. 4,4′-Methylene diphenyl diisocyanate (MDI), *N*,*N*-dimethylformamide (DMF), ethylene glycol, zinc acetate dihydrate ($ZnC_4H_6O_4 \cdot 2H_2O$), and NaOH (97%) were brought from Shanghai Aladdin Reagent. Other rubber chemicals used were commercially available industrial products.

2.2. Preparation of MGO/ND/nanoZnO functional hybridized filler

The preparation process of the functional hybridized material is shown in Fig. 1. A total of 1.8 g GO was dispersed in 50 ml DMF through ultrasonic bath, and the suspension was purged using nitrogen for 20 min. MDI powder was added and the reaction was carried out for 24 h at 60 °C. The mixture was then rinsed using DMF, and any excessive MDI was removed. Finally, MGO was obtained after being treated with the coupling agent. Then, 0.2 g of ND was added in 50 ml of DMF to form a suspension after ultrasonic bath treatment. The ND was then added into the MGO solution and underwent 10 min ultrasonic treatment. The reaction proceeded at 60 °C, with the reaction product continuously stirred for 2 d. The solid products were collected after centrifugation and rinsed using DMF and deionized water at least five times. The MGO/ND complex (*i.e.*, ND adhered to MGO) was finally obtained.

The MGO/ND complex (1.8 g, 2.0 g) and $ZnC_4H_6O_4 \cdot 2H_2O$ (1.35 g, 2.70 g, 4.05 g, 5.39 g) were dispersed in 40 ml of ethylene glycol under ultrasonic treatment. Based on the reaction yield (the yield can reach 80% in the case of excessive sodium hydroxide),[38] in our experiment, sodium hydroxide was excessive. The mixture was heated to 120 °C while being stirred intensely. Sodium hydroxide, which was dissolved in distilled water, was added into the mixture. After 2 h of stirring, the mixture was cooled to room temperature, centrifuged, and rinsed using absolute ethyl alcohol and deionized water several times. The obtained product was freeze-dried to obtain the MGO/ND/nanoZnO functional hybridized fillers with different loading capacities of nanoZnO at 0.5, 1.0, 1.5, and 2.0 wt%, marked as MGO/ND/0.5 nanoZnO, MGO/ND/1.0 nanoZnO, MGO/ND/1.5 nanoZnO, and MGO/ND/2.0 nanoZnO, respectively. The specific surface area of the nano zinc oxide was measured by the N_2 adsorption–desorption method.

2.3. Preparation of NR/MGO/ND/nanoZnO composite material

The composition of the rubber composite material is shown in Table 1. The NR composite material was prepared through latex composite technology, where NR latex and a certain amount of filler suspension were mixed and stirred for 30 min. The latex mixture was then co-solidified immediately, using 0.5% $CaCl_2$ solution, and the solidified solid was dried to constant weight in an air-dry oven at 60 °C. The dried nanocomposite was incorporated with all kinds of rubber chemicals using an open-type, double-roller open mill at room temperature.

Other rubber ingredients (phr): stearic acid (4), accelerator D (0.5), accelerator M (2.21), accelerator DM (1.18), accelerator TMTD (0.32), anti-aging agent 4020 (1.5), sulfur (1.71).

2.4. Characteristic description

The ultrasonic cleaner used was a KQ-100KDB (Kunshan Ultrasonic Instruments Co., Ltd.). Fourier Transform Infrared Spectroscopy (FTIR, Nicolet 6700 Thermo Scientific Co., Ltd., USA) was employed to analyze the change of characteristic groups on the filler surface after hybridization. The chemical compositions of the filler before and after hybridization were analyzed by X-ray photoelectron spectroscopy (XPS, K-Alpha, Thermo Scientific Co. Ltd., USA). X-ray diffraction (XRD, X'Pert-Pro MPD, Panalytical) was performed at 25 °C, Cu target

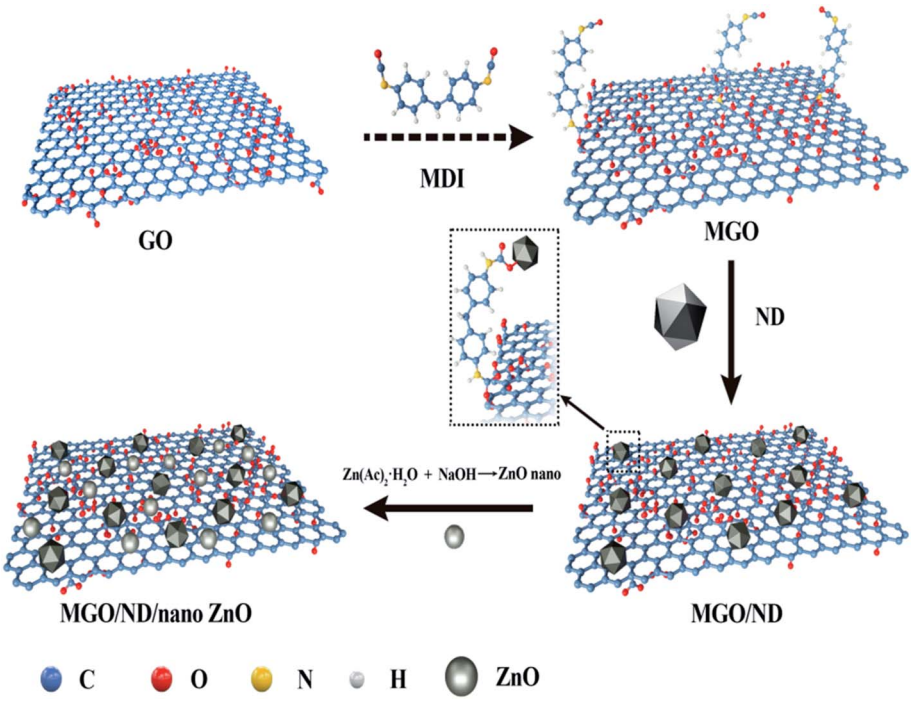

Fig. 1 Preparation process of hybrid functional filler.

Table 1 Composition of rubber composites[a]

Sample code ingredient (phr)	NR	GO	ND	Nano-ZnO	Common-ZnO
Pure NR	100	0	0	0	5
NR/GO	100	2	0	0	5
NR/MGO/ND	100	1.8	0.2	0	5
NR/MGO/ND/0.5 nanoZnO	100	1.8	0.2	0.5	4.5
NR/MGO/ND/1.0 nanoZnO	100	1.8	0.2	1	4
NR/MGO/ND/1.5 nanoZnO	100	1.8	0.2	1.5	3.5
NR/MGO/ND/2.0 nanoZnO	100	1.8	0.2	2	3

[a] Phr, parts per hundred of natural rubber by weight.

was operated under 40 kV and 30 mA, and XRD data were collected from 4° to 80° at rate of 4° min^{-1}. Thermogravimetric analysis (TGA, TGA5500, TA instrument) was used to investigate the thermal stability under nitrogen atmosphere at heating rate of 10 °C min^{-1}. Ultrasonic treatment of hybridized filler was carried out for 30 min, followed by observation of microstructures under transmission electron microscope (Tecnai G2 F20, FEI Co., Ltd., USA). A temperature-variable magnetic resonance crosslink density spectrometer (VTMR20-010V-I NiuMai, Analytical Instrument Co. China) was used to test the crosslink density of the vulcanized rubber, the measurement was performed at 60 °C, the sample was 10 cm long and 2 cm wide, the instrument's hydrogen test probe coil was 10 mm, the magnet strength was 0.5 T, and the magnet temperature was 35 ± 0.01 °C. Then, 0.5 g of unvulcanized rubber compound sample cut into small pieces were soaked in toluene solution in a clean copper mesh of known quality at room temperature, which was replaced every 24 h for 72 h, and then soaked in acetone solution for 24 h to extract the methylbenzene in the specimen. The undissolved product was then dried to constant weight at 60 °C. The content of bonded rubber in the specimen was then calculated, based on the following formula:

$$w = \frac{w_1 - (w_2 - w_3)}{w_1} \times 100\% \quad (1)$$

where w – content of bonded rubber, w_1 – rubber mass content in the specimen, w_2 – specimen mass, and w_3 – the mass after drying to constant weight.

A swelling test was performed on the vulcanizate in toluene solvent, according to the GB/T 7763-1987 standard. Two complete samples (40–50 mg) were immersed in toluene at 30 °C for 4 hours, and the weights of the samples were measured after swelling. The swelling index of vulcanized rubber was measured according to the following formula; two specimens were measured for every case and the average values were taken:

$$SI = \frac{W_b}{W_a} \quad (2)$$

where SI – swelling index, W_a – sample mass before swelling, and W_b – sample mass after swelling.

A universal testing machine (Hegewald & Peschke Co., Ltd., Germany) was used to measure the tensile strength and tear resistance of the rubber composite material at uniform crosshead velocity of 500 mm min^{-1}, according to the GB/T528-1998 and GB/T529-1999 standards. The sample was obtained at a vulcanization temperature of 150 degrees. The vulcanization characteristic curves of the specimens under different temperatures were tested by MDR (MD-3000, High Speed Rail Technology Co., Ltd., China), according to the GB/T16584-1996 standard. To investigate the vulcanization kinetics of the rubber composites, the vulcanization degree α at a specific time is calculated through the data obtained by the rotor-less vulcameter, which is defined as follows:

$$\alpha(t) = \frac{M_t - M_L}{M_H - M_L} \quad (3)$$

where M_H and M_L are maximum and minimum torques of the mixture under vulcanization temperature, respectively, and M_t is the torque at a given time t. The vulcanization rate can be defined as $d\alpha/dt$ and is calculated as follows:

$$\frac{d\alpha}{dt} = \frac{1}{M_H - M_L}\frac{dM}{dt} \quad (4)$$

3. Results and discussion

3.1. Structure and morphology of functional hybridized filler

The FT-IR graph of the filler is shown in Fig. 2(a). Pure GO had a characteristic peak of hydroxyl (–OH) at 3405 cm^{-1} and a characteristic peak of carbonyl (C═O) at 1730 cm^{-1}. Compared with pure GO, MGO had a new peak at 2870 cm^{-1}, corresponding to the alkyl group (–CH_2) of the coupling agent.[39] The (–NCO) peak (2230 cm^{-1}) in MGO had disappeared, indicating that the aminoester reaction had occurred. A new (–NH–) stretching vibration peak appeared at 3309 cm^{-1}, which further proved that MDI had been grafted onto GO. In addition, the new (–C═O) stretching vibration peak of MGO appeared at 1644 cm^{-1}, which also proved that MDI was successfully grafted onto GO. According to the IR spectrogram of the MGO/ND/nanoZnO functional hybridized filler, a characteristic peak of ZnO appeared near 500 cm^{-1}.[40] Therefore, ZnO was successfully loaded onto the MGO/ND complex.

XPS testing was performed to further determine the chemical composition at the surface of the functional hybridized filler; the results are shown in Fig. 2(b). Additionally, the elemental quantitative analysis of hybrid fillers is shown in

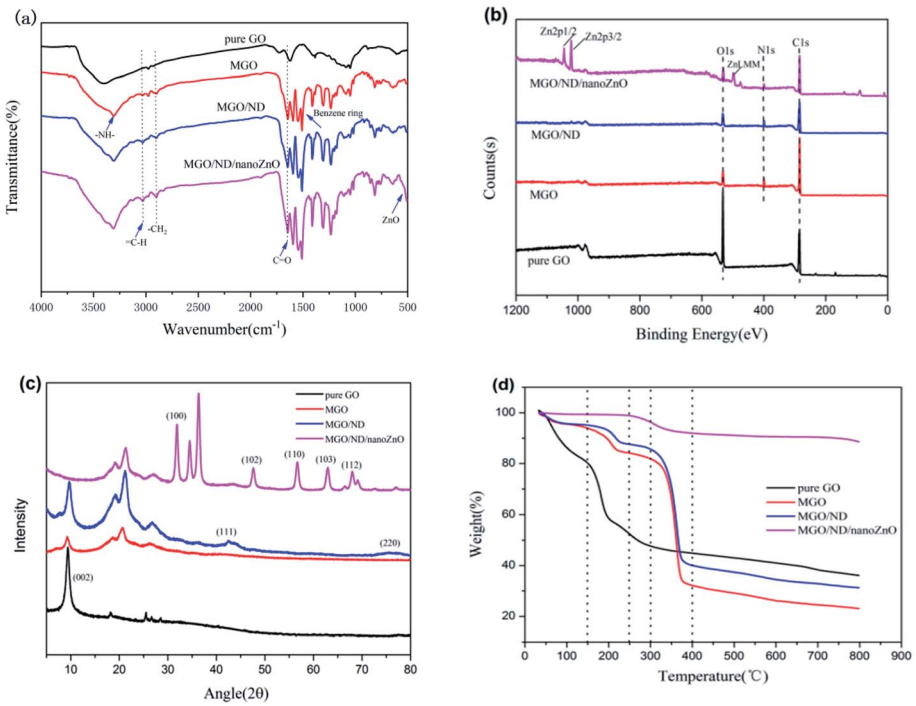

Fig. 2 (a) FT-IR spectra, (b) XPS survey spectra, (c) X-ray diffraction pattern spectra, and (d) TGA of GO, MGO, MGO/ND, and MGO/ND/nanoZnO under nitrogen.

Table 2 Elemental composition of each filler

Sample code element (%)	C	O	N	Zn
GO	48.21	51.79	0	0
MGO	71.95	20.97	7.08	0
MGO/ND	67.9	24.25	7.85	0
MGO/ND/nanoZnO	27.82	9.69	3.15	59.34

Table 2. MDI contained nitrogen, the N 1s peak was detected on the XPS graphs of MGO and MGO/ND, and the content of carbon increased and the content of oxygen decreased, corresponding to the reaction of the –NCO functional group, further proving the successful grafting of MDI. Fig. 3(a) and (b) show high-resolution single-scanning graphs of MGO and MGO/ND in N 1s region. Both specimens had two peak values under 398.7 and 399.5 eV, which correspond to –N=CO and N–C=O groups, respectively. Compared with that in MGO, the –N=CO peak area in MGO/ND was reduced, to some degree, due to the further reaction of –OH and –N=CO groups on the ND surface. This finding indicates that the coupling agent MDI successfully linked GO and ND.[41] Three characteristic peaks of Zn appeared on the XPS graph of the MGO/ND/nanoZnO functional hybridized filler, and the zinc content accounted for a large proportion of the same quality, further confirming that nanoZnO was successfully loaded onto the surface of MGO/ND complex through the wet chemical method.

The XRD graph is shown in Fig. 2(c). A new peak appeared in the MGO spectrum at 20°–30°, which corresponds to the structure formed by the grafting of MDI molecules onto GO. (111) and (220) peaks on the MGO/ND graph were characteristic planes of ND,[37] proving that ND was successfully grafted from MDI onto the GO. The original characteristic peak and sheet spacing of GO were $2\theta = 9.6°$ and $d = 0.92$ nm, respectively. After the MDI molecules were grafted onto GO sheets, the characteristic peak and sheet spacing of the MGO complex were $2\theta = 9.3°$ and $d = 0.95$ nm, respectively. The average particle size of ND was 5–7 nm, which is too large to be inserted between the GO layers. Consequently, the d-spacing (0.95 nm) of the MGO/ND did not change significantly. After nanoZnO was loaded onto the MGO/ND complex, the MGO/ND/nanoZnO functional hybridized filler had numerous XRD peaks characteristic of ZnO;[42] however, the characteristic peak of GO disappeared, possibly because nanoZnO exhibited a coating effect and uniformly covered the MGO/ND surface.

Considering the TGA under nitrogen data shown in Fig. 2(d), a mass loss of about 17% below 150 °C was observed, due to the evaporation of adsorbed water molecules. The most significant weight loss (about 40%) was observed between 150–200 °C, due to the pyrolysis of unstable oxygen-containing groups on the GO sheet. From 200 to 800 °C, about 20% of the mass loss was found to be caused by the pyrolysis of the carbon skeleton of GO. MGO and MGO/ND had almost no thermal weight loss below 150 °C, due to the large removal of adsorbed water during the preparation of MGO; the weight loss mainly occurred at about 150–250 °C (about 17%) and 250–400 °C (about 35%). This was due to the pyrolysis of residual oxygen-containing groups and MDI molecules, as well as the degradation of the GO carbon skeleton. The very small weight loss of MGO/ND/nanoZnO between room temperature and 250 °C was due to

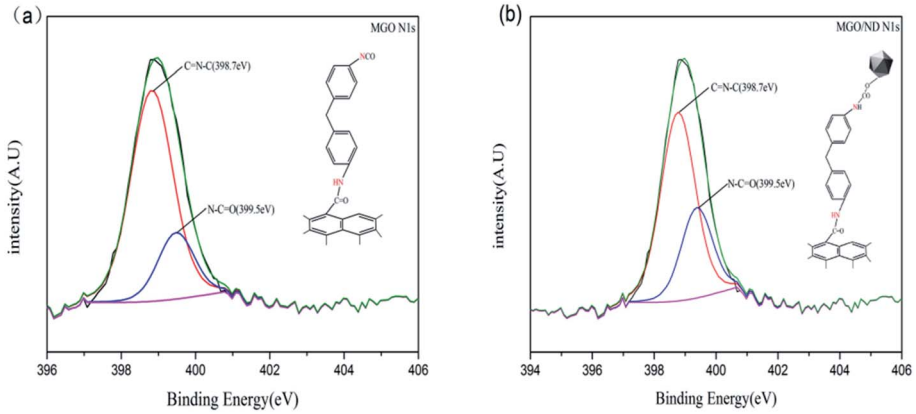

Fig. 3 Elemental composition of each filler, (a) MGO, and (b) MGO/ND.

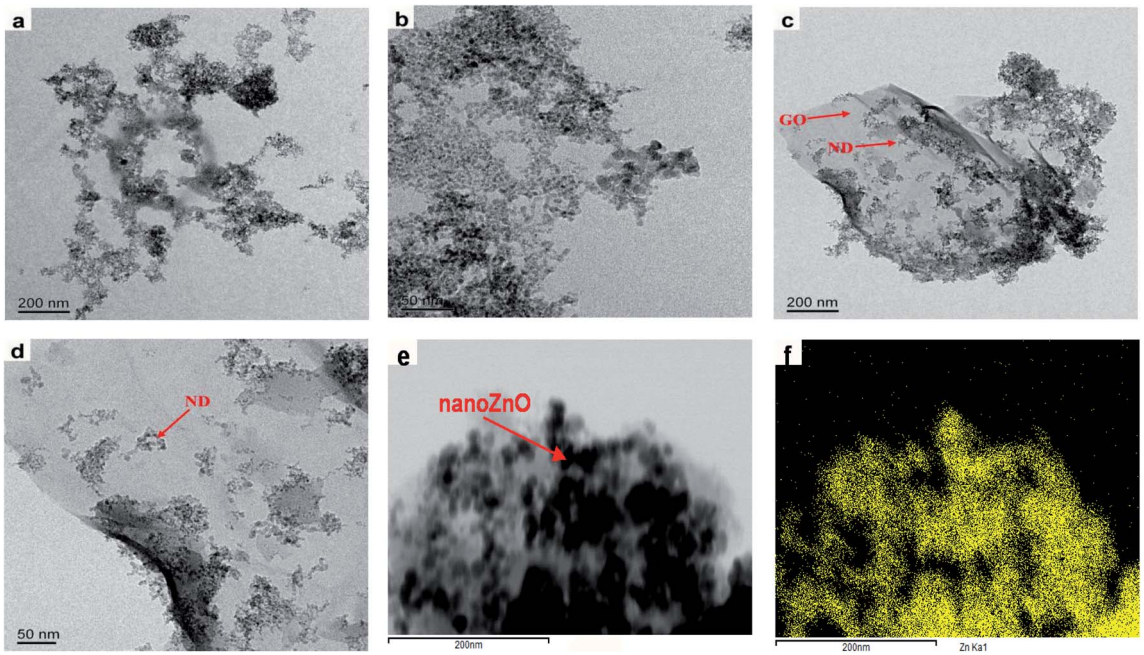

Fig. 4 TEM images of (a) the pristine ND nanocluster, (b) magnified ND, and (c) MGO/ND, magnified (d) MGO/ND and (e) MGO/ND/nanoZnO, and (f) zinc element mapping.

the evaporation of bound water, while the thermal weight loss between 250–800 °C was due to the pyrolysis of MDI molecules and the carbon skeleton. Nano zinc oxide has good thermal stability as a metal oxide. After densely attaching to the GO plate, the MGO/ND/nanoZnO hybrid functional filler had better thermal stability below 300 °C.

Fig. 4 shows the TEM graph of the functional hybridized filler. Single ND has a particle size of 5–7 nm. The particles showed intense aggregation tendency, being able to aggregate in solution and polymer matrix, and could bear ultrasonic treatment, as shown in Fig. 4(a) and (b).[43] Fig. 4(c) and (d) show that the ND particles were well-adhered to the corrugated GO surface. Fig. 4(e) and (f) show the TEM graph regarding nano-ZnO loading onto MGO/ND complex and the mapping graph of Zn. Zn uniformly covered the GO surface, certifying that nano-ZnO was successfully deposited onto the GO sheets.

3.2. Distribution of functional hybridized filler in natural rubber matrix

Fig. 5 shows the TEM images of vulcanized rubbers with different formulations. Fig. 5(a) and (b) are the TEM images of NR/MGO and NR/MGO/ND vulcanized rubbers, respectively. As shown in the figure, there are smaller zinc oxide particles aggregated in NR/MGO/ND vulcanized rubber. The presence of ND can effectively inhibit the aggregation of GO sheets, thereby improving the distribution of ordinary zinc oxide in the matrix. Fig. 5(c) and (d) are TEM images of NR/MGO/ND/1.0 nanoZnO and NR/MGO/ND/2.0 nanoZnO composite rubbers, respectively. It can be seen from the figure that after loading nano zinc oxide

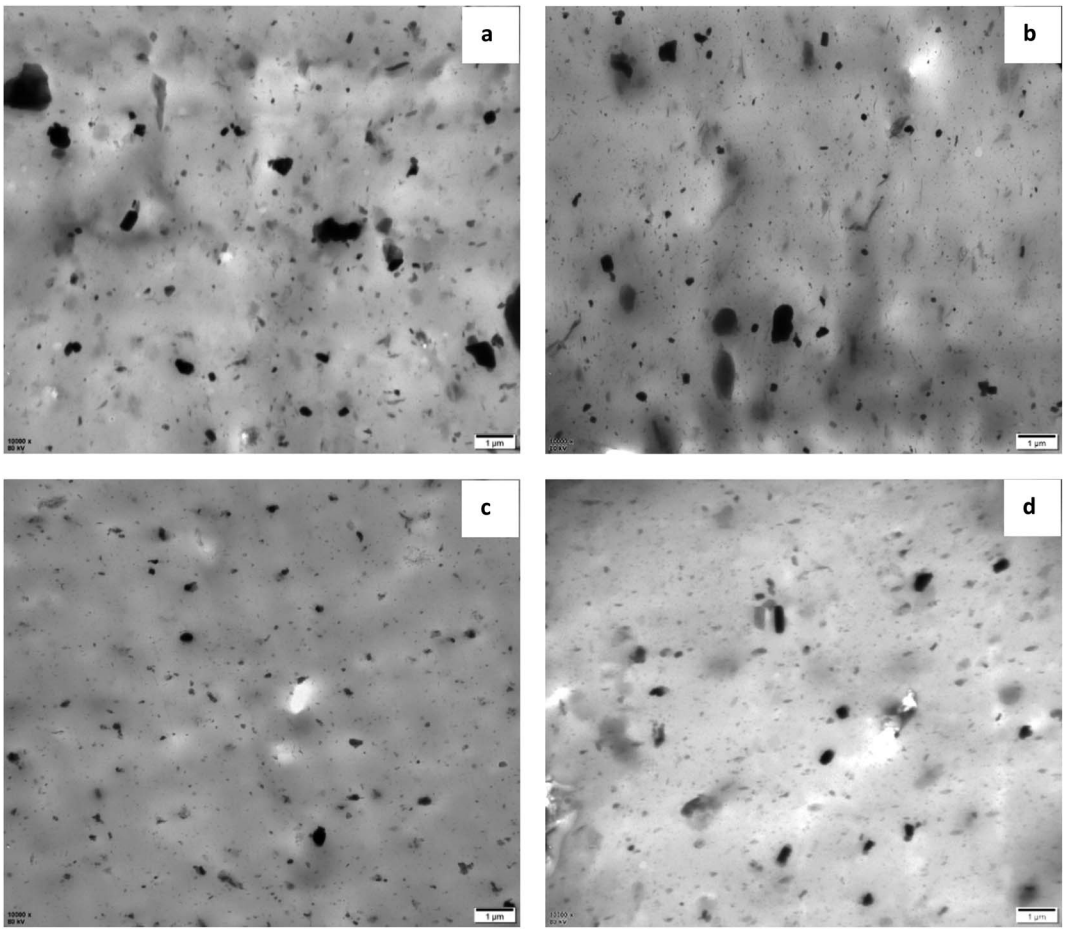

Fig. 5 TEM images of vulcanized rubber with different formulations, (a) NR/MGO, (b) NR/MGO/ND, (c) NR/MGO/ND/1.0 nanoZnO, (d) NR/MGO/ND/2.0 nanoZnO.

on MGO/ND, not only the use of ordinary zinc oxide is reduced, but also the distribution of nano zinc oxide is promoted, so that the particle size of zinc oxide in rubber composite is significantly smaller, and the distribution of the filler is more uniform. With the increase of nano zinc oxide loading to 2.0 phr, the particle size of zinc oxide aggregates increased slightly. Obviously, excessive nano zinc oxide will increase the tendency of agglomeration. Therefore, the loading amount of nanoZnO should not be too large.

3.3. Vulcanization behaviors of rubber composite material

3.3.1. Vulcanization characteristics. The three research methods for rubber vulcanization are as follows: (1) physical–chemical methods, wherein a determined concentration of vulcanizing agent changes with crosslinking time. The deficiency of this method lies in unreliable content determination of the vulcanizing agent. (2) Thermal analysis methods, in which the DSC technology is based on the following hypothesis: reaction heat is only caused by crosslinking reactions and is in direct proportion to the crosslinking reaction degree. For complicated reaction systems, however, this hypothesis lacks evidence.[2] (3) Vulcameter methods, which can conveniently acquire various parameters in the rubber vulcanization process and, through analysis, these data can reflect the time-dependent change of rubber curing degree under a constant temperature. This method was adopted in the present experiment.

Fig. 6 shows the vulcanization curves of different rubber composite materials under four different temperatures. The rubber vulcanization process is well-known to be divided into the following three phases: scorching period, crosslinking period, and reversion period. The scorching period involves the crosslinking precursor formation process of sulfur and various rubber chemicals under a certain temperature. During this period, effective crosslinking is not formed; thus, the torque will not change, which signifies a safe processing period. The crosslinking period involves the reaction process between the crosslinking precursor formed in the previous period and active sites on the rubber chain, wherein the torque (as measured by a rheometer) increases to a maximum value during this period. The reversion period refers to the fracturing process of multi-sulfur bonds (R–S_x–R) formed in the crosslinking period, which results in poor physical properties of the resultant vulcanized rubber. Fig. 6(d) shows that, under high temperatures, the curing curve presents an obvious reversion phenomenon during vulcanization, where addition of the filler does not influence this phenomenon. It has been shown that the cause for this reversion phenomenon is the facilitating effect of high

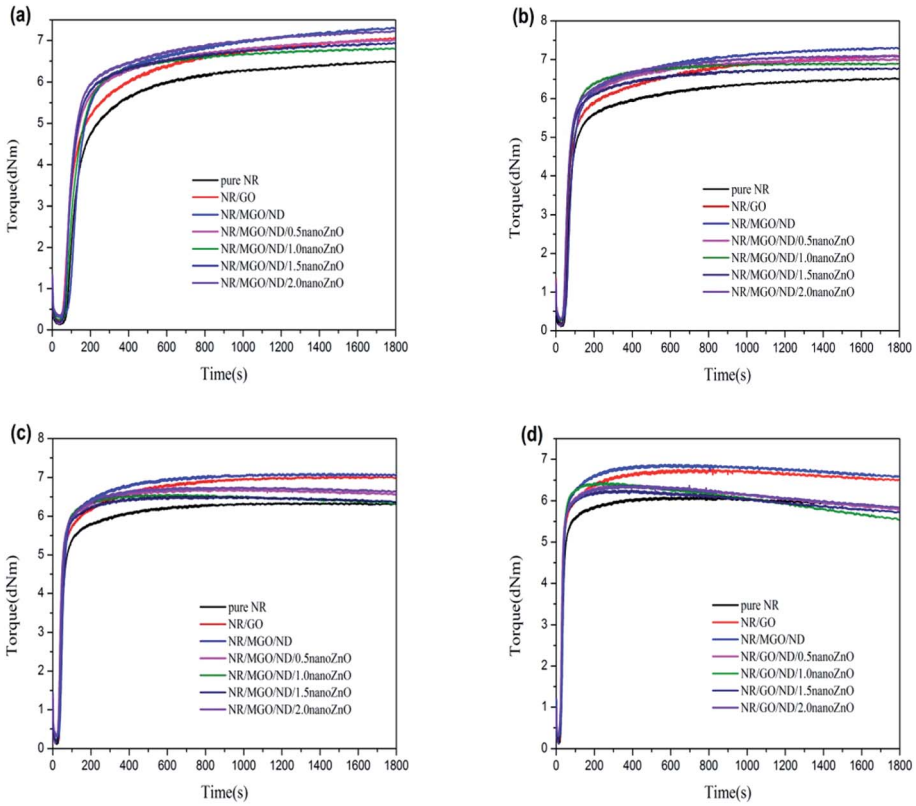

Fig. 6 MDR curves of rubber composites at different vulcanization temperatures: (a) 130 °C, (b) 140 °C, (c) 150 °C, and (d) 160 °C.

temperatures on the desulfurization reaction; namely, multisulfur bonds are easily formed in the crosslinking period fractures under high temperatures.[44,45]

Fig. 7 shows the effects of temperature and different functional hybridized fillers on the scorch time (t_{10}) and optimum curing time (t_{90}) of the rubber composite material. The results show that both the scorch time and optimum curing time of the rubber composite material have an evident temperature dependence. The scorch time of both specimens tended to be identical under high temperatures, as well as their optimum curing time. As previously reported, scorch time is generally dominated by the accelerating activity of the accelerant under vulcanization temperature and mobility of the rubber chain.[46] MGO/ND, which had good dispersity in the rubber matrix, effectively inhibited the flow of rubber chains and, thus, more heat had to accumulate to make the chain move. Thus, the NR/MGO/ND composite material had the longest scorch time. The shortening of scorch time after nanoZnO loading was associated with the higher accelerating activity of nanoZnO. The influence of temperature on optimum curing time was more remarkable than that on scorch time, where the long optimum curing time of the NR/GO composite material might be related

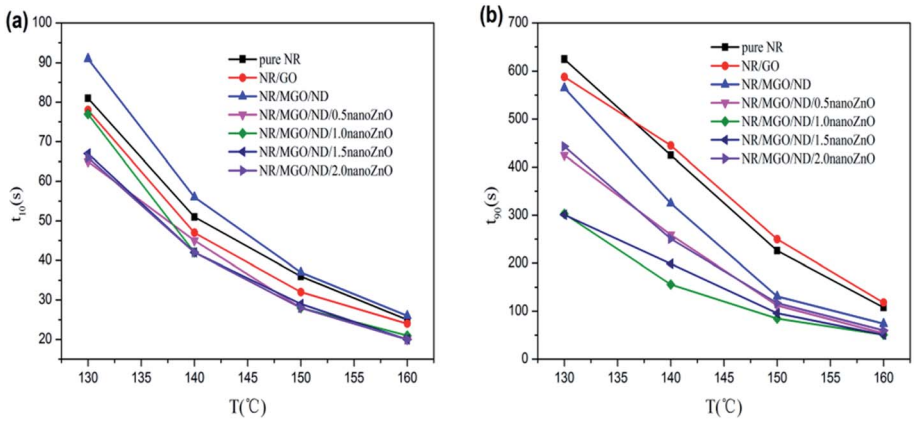

Fig. 7 Vulcanization data for rubber composites: (a) t_{10} and (b) t_{90}.

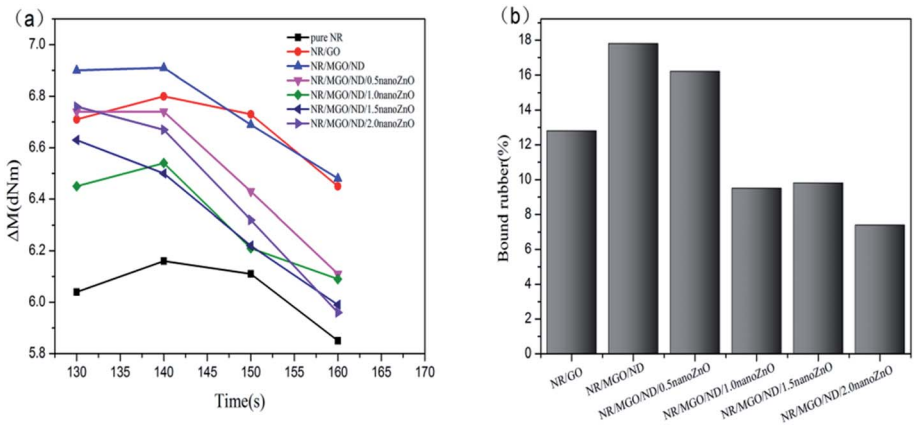

Fig. 8 (a) Effective torque and (b) bound rubber of the samples.

Table 3 Swelling degree and crosslink density of vulcanizate (1–7 are pure NR, NR/GO, NR/MGO/ND, NR/MGO/ND/0.5 nanoZnO, NR/MGO/ND/1.0 nanoZnO, NR/MGO/ND/1.5 nanoZnO, and NR/MGO/ND/2.0 nanoZnO, respectively.)

	1	2	3	4	5	6	7
Crosslink density (10^{-4} mol cm^{-3})	2.11	2.38	2.54	2.44	2.17	2.13	2.12
SI (%)	4.33	4.19	3.72	4.06	4.24	4.21	4.29

to adsorption of accelerants onto the GO by active groups.[47] Interestingly, the MGO/ND complex reduced the optimum curing time of vulcanized rubber. Based on analysis, this reduction was correlated with the high bound rubber content in the NR/MGO/ND composite material. In general, no rubber chemicals existed in the bound rubber, and high content of bound rubber means increased content of accelerant in the matrix, which serves to promote vulcanization. Another possible reason was that the MGO/ND complex enlarged the heat conductivity of rubber under vulcanization temperature, accelerated heat transfer, and then elevated the vulcanization rate.[19]

Fig. 8(a) displays the effect of various fillers on effective torque of vulcanized rubber. The effective torque declined under high temperature (160 °C), which was accompanied by a notable reversion phenomenon. The NR/MGO/ND composite material led to the maximum effective torque for the whole process. After *in situ* nanoZnO loading, the effective torque decreased.

Effective torque is measured as a value of crosslink density in the vulcanized rubber; in addition, crosslink density is an important parameter of vulcanized rubber, which mainly depends on the contents of sulfur and accelerant in the matrix, as well as the ratio of accelerant content to sulfur content.[48–50] Moreover, crosslink density has a great impact on the modulus and mechanical properties of vulcanized rubber.[51] In general, effective crosslink density in the rubber nanocomposite material involves the chemical crosslinking action of sulfur bonds between rubber chains and the possible physical entanglement (*i.e.*, physical crosslinking) between rubber chains; this interaction does not cause decreased effectiveness in the deformation process.[52] The crosslink density and swelling degree of each rubber composite material, as measured by a low-field nuclear magnetic crosslink density meter and the swelling experiment, are shown in Table 3. Based on formula (1), the bound rubber content of each mixed rubber was measured, as shown in Fig. 8(b) below.

Table 3 shows that the addition of filler increased the crosslink density of natural rubber, and that the swelling index also changed with crosslink density. Swelling of the vulcanizate is caused by the penetration of solvent molecules into the gaps

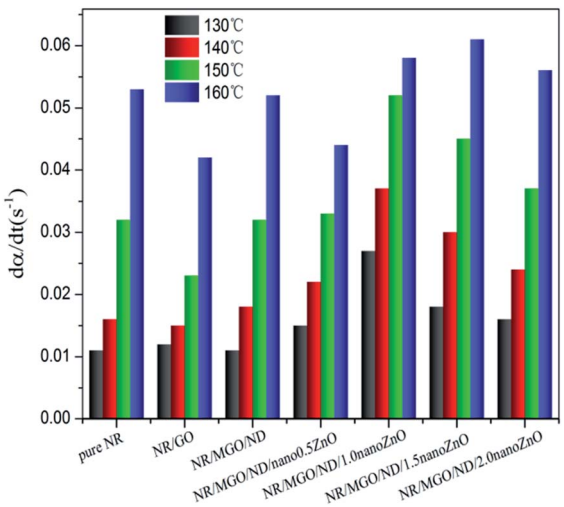

Fig. 9 Maximum vulcanization rate of rubber composites at different temperatures.

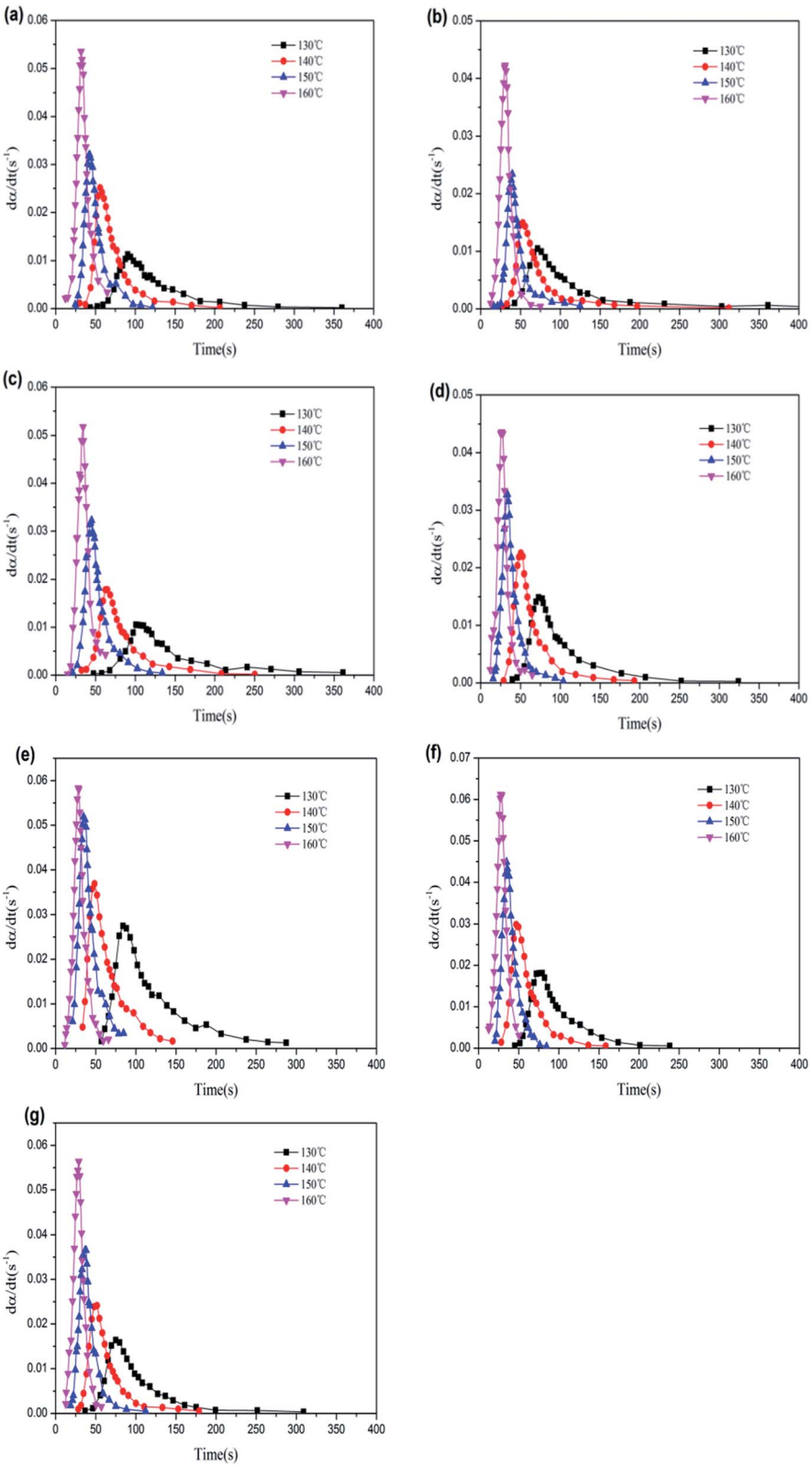

Fig. 10 Relationship between vulcanization rate and time of rubber composites: (a) pure NR, (b) NR/GO, (c) NR/MGO/ND, (d) NR/MGO/ND/0.5 nanoZnO, (e) NR/MGO/ND/1.0 nanoZnO, (f) NR/MGO/ND/1.5 nanoZnO, and (g) NR/MGO/ND/2.0 nanoZnO.

between the rubber molecules. The greater the crosslink density of the rubber, the more crosslink points between molecular chains per unit length, which limits the expansion of the rubber chain caused by extensibility, making it difficult for the solvent to penetrate into the gap between the rubber chains, thereby reducing the expansion index.[53] The vulcanized rubber with

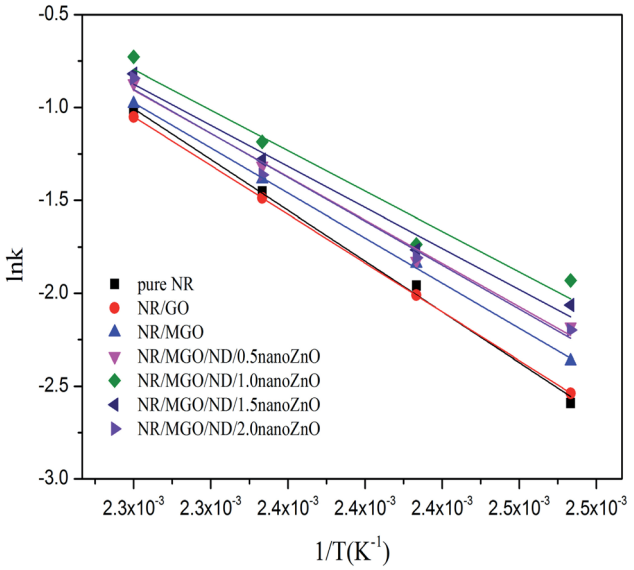

Fig. 11 Fit curve of ln *k* and 1/*T*, according to the Arrhenius function.

MGO/ND added had the maximum crosslink density, which increased by about 20% in comparison with that of pure natural rubber; at the same time, its swelling index was the smallest, which maintained a corresponding relationship with the crosslink density. The data of bound rubber in Fig. 8(b) show that the specimen with MGO/ND complex added had the maximum content of bound rubber, which indicates that the interaction between MGO/ND and the NR matrix is the strongest, as the ND particles inhibited the aggregation of GO sheets in the natural rubber matrix, making MGO/ND more dispersible in the NR matrix. However, after nanoZnO was loaded onto the MGO/ND complex, the content of bound rubber declined. The reason for this was that nanoZnO coated the MGO/ND complex and weakened the interfacial interaction between the rubber matrix and filler, thus decreasing the content of formed bound rubber.

3.3.2. Vulcanization kinetics. Fig. 9 shows the maximum vulcanization rates of all vulcanized rubbers under four temperatures. Different fillers were shown to exert different effects on the vulcanization rate of natural rubbers under different temperatures. When the Zn content was kept identical, the functional hybridized fillers loaded with nanoZnO all presented facilitating effects on vulcanization. The optimal loading capacity of nanoZnO was 1 wt%; this value was ascribed to high activity by virtue of the high specific surface area of nanoZnO. Therefore, nanoZnO particles could more effectively adsorb stearic acid and accelerant into the natural rubber matrix,[54] improve the generation efficiency of crosslinking precursors, greatly increase the reaction probability between crosslinking precursor and rubber chain,[55] and elevate the vulcanization

Table 4 Kinetic parameters of each rubber sample

			Reaction order			
Sample code	Temp. (°C)	*K*	*m*	*n*	*E* (kJ mol^{-1})	R^2
Pure NR	130	0.075	0.84	3.74	75.78	0.99
	140	0.141	0.80	2.56		
	150	0.234	0.93	2.39		
	160	0.357	1.03	1.97		
NR/GO	130	0.080	0.84	3.16	77.42	0.99
	140	0.134	0.13	3.94		
	150	0.226	1.07	2.81		
	160	0.350	1.11	2.17		
NR/MGO/ND	130	0.094	1.02	2.77	67.01	0.99
	140	0.159	1.02	2.76		
	150	0.250	1.00	2.41		
	160	0.376	1.09	2.05		
NR/MGO/ND/0.5 nanoZnO	130	0.113	0.86	2.97	64.44	0.98
	140	0.161	0.87	2.67		
	150	0.269	1.08	2.31		
	160	0.419	1.33	2.01		
NR/MGO/ND/1.0 nanoZnO	130	0.145	0.72	2.52	60.22	0.96
	140	0.177	0.71	2.18		
	150	0.306	0.90	2.02		
	160	0.483	1.01	2.75		
NR/MGO/ND/1.5 nanoZnO	130	0.127	0.85	2.70	61.14	0.97
	140	0.171	0.18	2.31		
	150	0.278	0.92	2.04		
	160	0.441	1.18	1.76		
NR/MGO/ND/2.0 nanoZnO	130	0.111	0.85	2.62	65.44	0.98
	140	0.164	0.86	2.48		
	150	0.256	0.98	2.15		
	160	0.431	1.19	1.85		

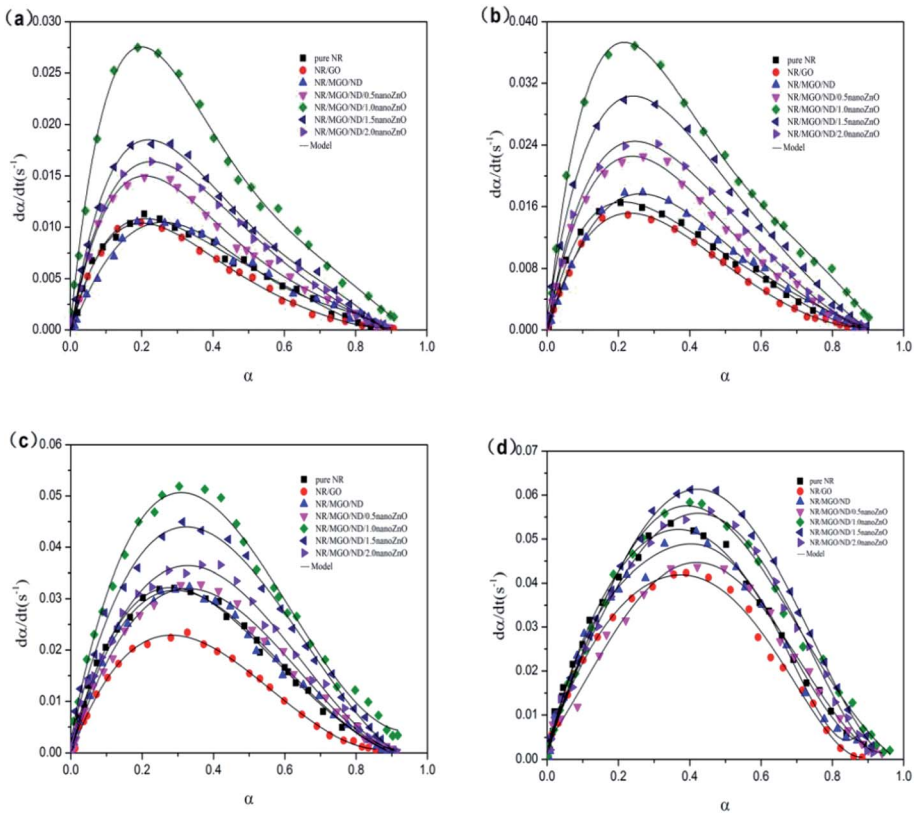

Fig. 12 Relationship between vulcanization rate and conversion rate at (a) 130 °C, (b) 140 °C, (c) 150 °C, and (d) 160 °C.

rate. This finding fully certifies that nanoZnO has a better vulcanization-promoting effect than traditional ZnO.

Fig. 10 gives the corresponding relationship between the vulcanization rate of rubber composites and time under different vulcanization temperatures. Vulcanization rates of all specimens were shown to firstly increase and then decrease with vulcanization time, accompanied by notable autocatalytic behavior, which could be explained by the competition between the vulcanization reaction dominated by chemical means and the vulcanization reaction dominated by physical means (*i.e.*, viscosity increase). As predicted by the autocatalysis equation, the maximum reaction rate appeared at any time (except for the start of the reaction) as, during this chemical reaction process, the rubber vulcanization degree was not only related to both the unreacted sulfur and accelerant, but also to the multi-sulfur bonds formed by crosslinking.[56]

Many dynamical models describing the autocatalysis process have been used in related reports.[57,58] The common Kamal–Sourour model used to describe the vulcanization kinetics is defined as follows:[59]

$$\frac{d\alpha}{dt} = k(T)\alpha^m(1-\alpha)^n \quad (5)$$

where m and n are reaction orders, T is the absolute temperature, and k is the rate constant, which is also an Arrhenius function of the absolute temperature T, expressed as

$$\ln k(T) = \ln A - \frac{E}{RT} \quad (6)$$

where R is a general gas constant, A is a pre-exponential factor, and E is the activation energy of the optimum curing process, which can be obtained by drawing a figure for $1/T$ through $\ln k$, as shown in Fig. 11. The values of $k(T)$, m, n, and E, for all specimens, were fitted and calculated by non-linear regression. The results are listed in Table 4.

Table 4 shows that the addition of the functional hybridized filler reduced the activation energy of the rubber composite in the optimum curing period. Correspondingly, the vulcanization rate constant was enlarged, due to the high surface activity of nanoZnO; its facilitating effect on rubber vulcanization was remarkably superior to that of traditional ZnO. The vulcanization rate declined when the *in situ* loading capacity of nanoZnO was greater than 1 wt%. Thus, the optimal loading capacity of nanoZnO must be applied to realize the vulcanization-facilitating effect of the functional hybridized filler; this ability might be related to the aggregation of nanoZnO particles. In summary, the kinetic mechanism of rubber vulcanization is complicated and related to other causes (*e.g.*, chemical catalytic action of the filler).

Fig. 12 shows the $d\alpha/dt$–α relation curves of rubber composite materials under four temperatures. The reaction rate of the rubber composite material increased with the conversion rate at the beginning of the crosslinking period and reached a maximum value within 0.2 to 0.4, which was consistent with the autocatalysis model mentioned previously. Therefore, the experimental data were in good agreement with the model that we selected.

Table 5 Mechanical properties of various rubber composites

Sample code	Tensile strength (MPa)	Tear strength (MPa)	Elongation break (%)	Stress at 100% strain (MPa)	Stress at 300% strain (MPa)
Pure NR	11.39	25.23	458.86	0.99	2.71
NR/GO	11.95	25.58	516.70	1.06	2.82
NR/MGO/ND	6.34	26.99	365.09	1.38	4.23
NR/MGO/ND/0.5 nanoZnO	15.57	31.73	523.65	1.02	3.03
NR/MGO/ND/1.0 nanoZnO	18.16	31.47	543.19	1.08	3.11
NR/MGO/ND/1.5 nanoZnO	21.34	33.34	534.36	1.09	3.31
NR/MGO/ND/2.0 nanoZnO	23.15	33.22	529.57	1.16	3.54

3.4. Mechanical properties of vulcanized rubber

The mechanical properties of vulcanized rubber are listed in Table 5. In general, the interaction between matrix and filler,[60] and whether a network is formed between the matrix and the filler are important determinants of the mechanical properties of composite materials. As ND inhibits the aggregation of GO sheets, the dispersibility is improved, the elongation at break of NR/MGO/ND specimen declined, and the tensile strength increased, indicating that the composite rigidity was improved, to a certain degree. The tensile strength, tear strength, elongation at break, 100% stretching strength, and 300% stretching strength of the NR/MGO/ND/1.0 nanoZnO specimen, with the best vulcanization performance, were increased by 59%, 25%, 18%, 9%, and 14%, respectively.

4. Conclusions

ND and nanoZnO particles were added onto the surface of GO through chemical grafting and physical deposition, respectively, to prepare a MGO/ND/nanoZnO functional hybridized material for use in the latex composite method with GO as the carrier and 4,4′-methylene diphenyl diisocyanate (MDI) as the coupling agent. A vulcanization kinetics study indicated that the vulcanization of natural rubber conformed to the autocatalysis model, where pure GO had only a minor influence on the vulcanization behaviors of natural rubber. Meanwhile, the MGO/ND complex shortened the optimum curing time of natural rubber. When 1 wt% nanoZnO was loaded onto the MGO/ND complex, the activation energy of the rubber composite decreased by 16% in the crosslinking period and the vulcanization efficiency was improved by approximately 63%. This phenomenon was associated with the favorable dispersity of the hybridized filler in the rubber matrix and its high surface activity. Furthermore, the tensile strength, tear strength, elongation at break, 100% stretching strength, and 300% stretching strength of the NR/MGO/ND/1.0 nanoZnO specimen were elevated by 59%, 25%, 18%, 9%, and 14%, respectively, compared with those of pure NR. These results indicate that the prepared MGO/ND/nanoZnO functional hybridized filler can remarkably promote the vulcanization characteristics of natural rubber.

Conflicts of interest

There are no conflicts of interest to declare.

Acknowledgements

We gratefully acknowledge financial support from the National Natural Science Foundation of China (NSFC No. 51663003), Science and Technology Foundation of Guizhou Province (Grant No. [2019]2166).

Notes and references

1 J. E. Mark, B. Erman and M. Roland, *The science and technology of rubber*, Academic press, 2013.
2 R. Ding and A. I. Leonov, *J. Appl. Polym. Sci.*, 1996, **61**, 455–463.
3 L. M. Lopez, A. B. Cosgrove, J. P. Hernandez-Ortiz and T. A. Osswald, *Polym. Eng. Sci.*, 2007, **47**, 675–683.
4 A. Y. Coran, *Rubber Chem. Technol.*, 1965, **38**, 1–14.
5 E. Ehabé, F. Bonfils, C. Aymard, A. K. Akinlabi and J. Sainte Beuve, *Polym. Test.*, 2005, **24**, 620–627.
6 N. Rattanasom, A. Poonsuk and T. Makmoon, *Polym. Test.*, 2005, **24**, 728–732.
7 S. Mostoni, P. Milana, B. D. Credico, M. D'Arienzo and R. Scotti, *Catalysts*, 2019, **9**, 664.
8 A. Ansarifar, L. Wang, R. J. Ellis and Y. Haile-Meskel, *J. Appl. Polym. Sci.*, 2011, **119**, 922–928.
9 B. Panampilly and S. Thomas, *Polym. Eng. Sci.*, 2013, **53**, 1337–1346.
10 I. J. Kim, W. S. Kim, D. H. Lee, W. Kim and J. W. Bae, *J. Appl. Polym. Sci.*, 2010, **117**, 1535–1543.
11 S. P. Thomas, E. J. Mathew and C. V. Marykutty, *J. Appl. Polym. Sci.*, 2012, **124**, 3099–3107.
12 K. Roy, M. N. Alam, S. K. Mandal and S. C. Debnath, *J. Sol-Gel Sci. Technol.*, 2014, **70**, 378–384.
13 A. Moezzi, A. M. Mcdonagh and M. B. Cortie, *Chem. Eng. J.*, 2012, **185**, 1–22.
14 E. Tang, G. Cheng, X. Ma, X. Pang and Q. Zhao, *Appl. Surf. Sci.*, 2006, **252**, 5227–5232.
15 M. Gaca, J. Pietrasik, M. Zaborski, L. Okrasa, G. Boiteux and O. Gain, *Polymers*, 2017, **9**, 645.
16 A. Susanna, L. Armelao, E. Callone, S. Dirè, M. D'Arienzo, B. D. Credico, L. Giannini, T. Hanel, F. Morazzoni and R. Scotti, *Chem. Eng. J.*, 2015, **275**, 245–252.
17 A. Susanna, M. D'Arienzo, B. D. Credico, L. Giannini, T. Hanel, R. Grandori, F. Morazzoni, S. Mostoni, C. Santambrogio and R. Scotti, *Eur. Polym. J.*, 2017, **93**, 63–74.

18 Y. Lin, Y. Chen, Z. Zeng, J. Zhu, Y. Wei, F. Li and L. Liu, *Composites, Part A*, 2015, **70**, 35–44.
19 G. Heideman, J. W. M. Noordermeer, R. N. Datta and B. V. Baarle, *Kautsch. Gummi Kunstst.*, 2003, **12**, 650–656.
20 G. Heideman, J. Noordermeer, R. N. Datta and B. V. Baarle, *Macromol. Symp.*, 2006, **245**, 657–667.
21 L. T. Tam, N. X. Dinh, N. V. Cuong, M. V. Quy, T. Q. Huy, D. Ngo, K. MØlhave and A. Le, *J. Electron. Mater.*, 2016, **45**, 5321–5333.
22 T. H. Fatt, *Development of Graphene Oxide Based Functional Materials*, 2014.
23 B. Mensah, K. C. Gupta, G. Kang, H. Lee and C. Nah, *Polym. Test.*, 2019, **76**, 127–137.
24 J. Wu, W. Xing, G. Huang, H. Li, M. Tang, S. Wu and Y. Liu, *Polymer*, 2013, **54**, 3314–3323.
25 R. Scaffaro and A. Maio, *Chem. Eng. J.*, 2016, **308**, 1034–1047.
26 B. Yin, J. Wang, H. Jia, J. He, X. Zhang and Z. Xu, *J. Mater. Sci.*, 2016, **51**, 5724–5737.
27 Y. T. Park, Y. Qian, C. Chan, T. Suh, M. G. Nejhad, C. W. Macosko and A. Stein, *Adv. Funct. Mater.*, 2015, **25**, 575–585.
28 M. H. Delville and A. Taubert, *Hybrid Organic-Inorganic Interfaces: Towards Advanced Functional Materials*, John Wiley & Sons, 2018.
29 N. Rattanasom, T. Saowapark and C. Deeprasertkul, *Polym. Test.*, 2007, **26**, 369–377.
30 M. Acik, G. Lee, C. Mattevi, A. Pirkle, R. M. Wallace, M. Chhowalla, K. Cho and Y. Chabal, *J. Phys. Chem. C*, 2011, **115**, 19761–19781.
31 L. Zhang, K. Zhou, Q. Wei, L. Ma, W. Ye, H. Li, B. Zhou, Z. Yu, C. T. Lin, J. Luo and X. Gan, *Appl. Energy*, 2019, **233**, 208–219.
32 S. Rabiei and A. Shojaei, *Eur. Polym. J.*, 2016, **81**, 98–113.
33 X. Luo, X. Yu, Y. Ma, K. Naito and Q. Zhang, *Thermochim. Acta*, 2018, **663**, 1–8.
34 F. Zhao, R. Liu, X. Yu, H. Ding, X. Qu and Q. Zhang, *J. Nanosci. Nanotechnol.*, 2015, **15**, 5807–5815.
35 D. Ponnamma, S. H. Sung, J. S. Hong, K. H. Ahn, K. T. Varughese and S. Thomas, *Eur. Polym. J.*, 2014, **53**, 147–159.
36 M. M. Senna, R. M. Mohamed, A. N. Shehab-Eldin and S. Ei-Hamouly, *J. Ind. Eng. Chem.*, 2012, **18**, 1654–1661.
37 S. Varghese and J. Karger-Kocsis, *Polymer*, 2003, **44**, 4921–4927.
38 D. M. Khan, A. Kausar and S. M. Salman, *J. Macromol. Sci., Polym. Rev.*, 2015, **55**, 744–768.
39 Y. Zhang, K. Y. Rhee and S. J. Park, *Composites, Part B*, 2017, **114**, 111–120.
40 T. L. Thanh, Q. L. A. Bao and H. N. Huu, *Int. J. Nanotechnol.*, 2018, **15**, 108–117.
41 Y. Zhang and S. J. Park, *Composites, Part A*, 2018, **112**, 356–364.
42 D. Fu, G. Han, Y. Chang and J. Dong, *Mater. Chem. Phys.*, 2012, **132**, 673–681.
43 R. Martín, P. C. Heydorn, M. Alvaro and H. Garcla, *Chem. Mater.*, 2009, **21**, 4505–4514.
44 A. Khouider, J. Bouzon and J. M. Vergnaud, *Thermochim. Acta*, 1986, **98**, 285–299.
45 G. Milani, E. Leroy, F. Milani and R. Deterre, *Polym. Test.*, 2013, **32**, 1052–1063.
46 N. Z. Noriman, H. Ismail and A. A. Rashid, *Polym. Test.*, 2010, **29**, 200–208.
47 A. D. Falco, A. J. Marzocca, M. A. Corcuera, A. Eceiza, I. Mondragon, G. H. Rubiolo and S. Goyanes, *J. Appl. Polym. Sci.*, 2009, **113**, 2851–2857.
48 A. J. Marzocca, A. L. R. Garraza, P. Sorichetti and H. O. Mosca, *Polym. Test.*, 2010, **29**, 477–482.
49 A. J. Marzocca and M. A. Mansilla, *J. Appl. Polym. Sci.*, 2007, **103**, 1105–1112.
50 R. Hagen, L. Salmén and B. Stenberg, *J. Polym. Sci., Part B: Polym. Phys.*, 1996, **34**, 1997–2006.
51 Y. Lei, Z. Tang, L. Zhu, B. Guo and D. Jia, *Polymer*, 2011, **52**, 1337–1344.
52 M. A. López-Manchado, J. L. Valentín, J. Carretero, F. Barroso and M. Arroyo, *Eur. Polym. J.*, 2007, **43**, 4143–4150.
53 M. A. Kader and A. K. Bhowmick, *Polym. Degrad. Stab.*, 2003, **79**, 283–295.
54 Y. H. Chen, L. Deng, Z. B. Man and M. Yang, *Adv. Mater. Res.*, 2011, **236–238**, 1757–1760.
55 S. Akhlaghi, M. Kalaee, S. Mazinani, E. Jowdar, A. Nouri, A. Sharif and N. Sedaghat, *Thermochim. Acta*, 2012, **527**, 91–98.
56 G. Sui, W. H. Zhong, X. P. Yang and Y. H. Yu, *Mater. Sci. Eng., A*, 2008, **485**, 524–531.
57 H. S. Y. Hsich, *J. Appl. Polym. Sci.*, 1982, **27**, 3265–3277.
58 K. Jönsson and P. Flodin, *J. Appl. Polym. Sci.*, 1991, **43**, 1777–1787.
59 M. R. Kamal and S. Sourour, *Polym. Eng. Sci.*, 1973, **13**, 59–64.
60 S. R. Dhakate and O. P. Bahl, *Carbon*, 2003, **41**, 1193–1203.

